Facile synthesis of high-surface area platinum-doped ceria for low temperature CO oxidation

Suresh Gatla[1], Daniel Aubert[2], Valérie Flaud[3], Rémi Grosjean[2], Thomas Lunkenbein[4], Olivier Mathon[1], Sakura Pascarelli[1], Helena Kaper[2*]

[1]ESRF – The European Synchrotron, 71, avenue des Martyrs, 38000 Grenoble, France
[2] Laboratoire des Synthèses et Fonctionnalisation des Céramiques, UMR 3080, CNRS/Saint-Gobain CREE, 550, Ave Alphonse Jauffret, 84306 Cavaillon, France
[3] Institut Charles Gerhardt, UMR 5253, Université Montpellier 2, Place Eugène Bataillon 34095 Montpellier Cedex 5 – France
[4] Fritz-Haber-Institute of the MPG, Department of Inorganic Chemistry, Faradayweg 4-6, 14195 Berlin

[*]helena.kaper@saint-gobain.com

Abstract
Using a simple slow decomposition method of nitrate precursors, high-surface area platinum-doped ceria with a crystallite size of 9 nm can be prepared. The catalytic performance of the compound can be tuned by changing the reduction temperature under hydrogen (300°C, 500°C and 700°C). The catalyst treated at 300°C shows the best catalytic performance, being active at room temperature. The materials were analysed using a combination of structural characterization methods (X-ray diffraction (XRD), nitrogen physisorption, high angle annular dark field scanning transmission electron microscopy (HAADF-STEM)), surface sensitive methods (X-ray photoelectron spectroscopy (XPS), H_2-chemisorption and H_2-temperature-programmed reduction (TPR)) and X-ray absorption fluorescence spectroscopy (XAFS). HAADF-STEM and XAFS analysis suggests successful doping of platinum in the ceria lattice. After pretreatment at 300°C, the situation is slightly different. While no defined platinum nanoparticles can be identified on the surface, some platinum is in a reduced state (XPS, H_2-chemisorption).

Keywords
CO oxidation; platinum-cerium oxide catalyst; platinum-doped cerium oxide; oxidation state; heterogeneous catalysis

1. Introduction

Carbon monoxide oxidation is important in various applications such as removal of CO in car exhaust streams[1], CO removal from hydrogen in polymer electrolyte membrane fuel cells[2,3] and more recently also in the context of indoor air quality[4]. Platinum group metals (PGM) are often used as active catalysts for CO oxidation. However, due to the economic, social and ecologic costs of the PGMs, these metals should be employed as efficiently as possible. One method to increase the atom efficiency of noble metal catalysts is to reduce their size to the nanoscale, considering the fact that basically the atoms at the particle surface are involved in the catalytic process. Reducing the particle size to the nanoscale not only increases the atom efficiency, but additional catalytic effects can emerge (nanoclusters, single-atom catalysis)[5–8]. Consequently, more questions on the nature of the catalytic active species in the catalytic process arise.

Indeed, many factors can influence the catalytic activity including particle size, support characteristics, surface area, and oxidation state. The latter point has recently provoked a debate on the oxidation state of PGM catalysts in the literature. While formerly the metallic form was found to be the most active one[9–11], some recent studies demonstrate the superior activity of oxidized PGM catalysts[12,13]. For example, Hensen *et al.* studied Rh-nanoparticles of different sizes (between 1.6 and 8 nm) for CO oxidation using in-situ XAFS[13]. They attributed the superior catalytic activity of the smaller nanoparticles to changes in the oxidation state under working conditions, which are not observed for bigger nanoparticles.

One possibility to decrease the particle size is to directly integrate the noble metal in the support lattice in form of dopants. As early as the 1970s, researcher started to study noble-metal promoted perovskites for automobile exhaust catalysis[14,15]. More recently, the integration of noble metals in CeO_2 has been studied by Hedge's group using flame combustion for CO oxidation[16,17], de-NO_x catalysis[18] and water gas shift reactions[19]. While this approach allows at least for a partial integration of the noble metal in the cerium oxide lattice, the relatively high synthesis temperature (roughly 1500°C) leads to small surface areas (< 10 m^2/g)[17]. Other synthesis procedure for noble metal doped ceria include plasma-arc synthesis[20], microemulsion[21], sonochemistry[22] and hydrothermal methods[22,23].

Ab initio calculations show that doping CeO_2 with Pd or Pt enhances the oxygen storage capacity (OSC) through lattice distortions and increases the number of oxygen ion vacancies[24]. Tang *et al.* use density functional calculation to calculate the bond distances in the hypothetical case where one Ce atom is replaced by a platinum atom in the surface layer of cerium oxide[25]. The authors show that through elongation of the bond distances involving

the oxygen between Pt and Ce, the energy for the removal of this oxygen is decreased, thus facilitating the creation of oxygen ion vacancies.

In this work, we address the question of the catalytic activity of platinum-cerium oxide catalyst systems in the light of the current discussion concerning the oxidation state of platinum combined with doping of cerium oxide. The catalyst is synthesized by a simple slow decomposition route, leading to a high surface area material.

2. Materials and Methods

2.1 Synthesis of Catalysts

One-step synthesis of Pt_CeO_2_one

The Pt_CeO_2_one sample series was synthesized by slow decomposition of the respective nitrate precursor mixture. In a typical synthesis, 0.0933 g $Pt(NO_3)_2$ ((Heraeus) was added to a solution containing 12.5646 g $Ce(NO_3)_2$*$6H_20$ in isopropanol (100ml). After complete dissolution, the solvent was removed by rotational evaporation until nearly complete dryness. The resulting mixture was dried in an oven at 100°C for 48h. The powder was calcined using the following programme: RT-180°C(2h)-200°C(3h)-220°C(3h)-500°C (2h)

The platinum content was verified using ICP measurements, see SI2.

Synthesis of cerium oxide support

Pure cerium oxide was synthesized by decomposition of cerium nitrate. In order to be coherent with the one-step synthesis of Pt/CeO_2, pure cerium oxide was synthesized in the same manner. Thus, $Ce(NO_3)\cdot 6H_2O$ (Sigma Aldrich) was dissolved in isopropanol at room temperature. After complete dissolution, the solvent was removed by rotational evaporation at 60°C until nearly complete dryness. The resulting solid was dried at 100°C for 48h and crushed in a mortar. The powder was calcined using the following programme: RT-180°C(2h)-200°C(3h)-220°C(3h)-500°C (2h)

2.2 Catalytic Test

CO oxidation by molecular oxygen was carried out in a flow-through reactor. The total gas flow was kept constant to 10l/h. The composition of the gas was 6000 ppm of CO and 10 000 ppm of O_2, assuring oxidative conditions during the test. The grain size of the catalyst powder was kept between 150µm and 250µm. 200 mg of catalyst powder was put into the quartz reactor, giving a gas hourly space velocity of 50 000 h^{-1}. During the test, a heating ramp of 2°C/min was applied. The gases were analysed using gas chromatographe SCR 3000,

coupled with a TCD detector and equipped with two columns, MolSieve5APLOT and Column PLOT U. One measurement point takes two minutes. For the isothermal tests, the conditions were 25 mg of catalyst powder diluted in SiC, 2000 ppm of CO and 3000 ppm of oxygen and a total flux of 10l/h, resulting in a GHSV of 400 000 h^{-1}.

Pre-treatment of the catalyst under hydrogen was carried out in situ on the same set-up using 40% H_2 in Helium with a flow rate of 10l/h. The catalyst was heated to the desired temperature in 34 minutes and kept at that temperature for 2h.

2.3 Methods

XRD patterns were recorded on an X'Pert diffractometer from PANanalytical Instruments equipped with a CuKα monochromatic radiation source (40 kV, 35 mA). The crystallite size was determined using the Debye-Scherrer method. Lattice parameters were determined using High Score Plus.

Nitrogen physisorption was carried out at 77K using on a Micromeritics Tristar II instrument, after treatment of the samples under primary vacuum (20 mTorr) at 280 °C for four hours. Surface areas were calculated using the Brunauer Emmet Teller (BET) method over the range P/P0 = 0.07-0.30, where a linear relationship was maintained.

ICP-AES measurements were carried out on a Varian Vista Ax instrument.

H_2-chemisorption and H_2-TPR experiments were carried out on an Automated Catalyst Characterization System (Autochem II 2920, micromeritics). H_2-chemisorption was carried out at -77°C to avoid hydrogen spillover to ceria. For the experiment, 200 mg of catalysts were reduced at 300°C under 5%H_2/Ar with a flow rate of 30ml/min. The samples was flushed under He at 200°C for 1 h. The sample was cooled to -77°C and pulses of H_2 were applied until saturation. H_2-TPR measurements were carried out using the same system, on 200mg of catalyst powder. The samples were pretreated at 350°C under oxygen for 1h and then cooled to room temperature. Hydrogen uptake was measured with a heating rate of 5°C/min, from 20°C to 900°C under 5%H_2/Ar and a flow rate of 30ml/min.

The surface composition was monitored by X-ray photoelectron spectroscopy (XPS) on an ESCALAB 250 (Thermo Electron). The X-ray excitation was provided by a monochromatic Al Kα (1486.6 eV) source. The analyzed surface was 400 µm in diameter. The background signal was removed using the Shirley method[26]. The surface atomic concentrations were determined from photoelectron peaks areas using the atomic sensitivity factors reported by Scofield[27]. Binding energies (BE) of all core levels were referred to the C-C of C1s carbon at 284.8 eV.

High resolution transmission electron microscopy (HRTEM) micrographs and HAADF-STEM images were recorded on a FEI Titan 80-300 equipped with a Cs corrector.

XAFS experiments at Pt L_{III}-edge (11564 eV) were performed at the BM23 beam line of the European Synchroton Radiation Facility (ESRF, Grenoble, France). EXAFS spectra were recorded in fluorescence mode for the samples using a Ge multi element detector, whereas the transmission mode was used for reference compounds (Pt foil, PtO_2, $PtCl_2$ and $PtCl_4$). An ion chamber filled with 0.16 bar Ar was used to measure the incoming photon flux (I_0), whereas the emitted photons (I_1) were detected in the second ion chamber filled with 0.54 bar Ar. Eventually, the chambers were filled up to 2 bar with helium. A monochromatic X-ray beam was obtained from the white beam by using a Si(111) double crystal monochromator. Harmonic rejection has been performed using Si coated mirrors. The photon energy was calibrated with the edge energy (11564 eV) obtained from the maximum in the first derivative spectrum of Pt foil. The EXAFS parts of the spectra were collected with a constant step in photoelectron wave vector k, with $\Delta k = 0.05$ $Å^{-1}$ up to 12 $Å^{-1}$. For each sample, three consecutive EXAFS spectra have been collected and averaged for data analysis. The extraction of the EXAFS $\chi(k)$ function was done using Athena and fitting of the EXAFS was performed with Artemis software. Fourier transform of EXAFS function $\chi(k)$ into R space with k^3 weighted factor and Kaiser-Bessel window function has been performed in the range 2 to 12 $Å^{-1}$, yielding the function $|\chi(R)|$ ($Å^{-4}$). The Artemis input files containing the information on crystal structure, lattice parameters and space group were taken either from ATOMS data base or ICSD (Inorganic Crystal Structure Database).

For the hydrogen treated samples, the samples were treated ex-situ and pressed into pellets of 13mm of diameter.

3. Results and Discussion

3.1 X-ray diffraction and nitrogen physisorption

XRD analysis of the as-synthesized sample and samples treated under hydrogen are shown in Figure 1. All diffractograms can be indexed to phase-pure cerium oxide, the presence of Pt- or PtO_2 nanoparticles cannot be confirmed even after hydrogen treatment at 700°C. A sharpening of the peaks with increasing temperature can be observed, which is most dominantly for the temperature jump between 500°C and 700°C, indicating the growth of the cerium oxide crystals. The crystallite size and the lattice parameter of cerium oxide are presented in Table 1. After hydrogen treatment at 300°C and 500°C, the crystallite size (8-10 nm) and lattice

parameter remain stable. Increasing the hydrogen treatment temperature to 700°C significantly increases the crystallite size to 31 nm. One has to keep in mind that XRD analysis as often employed to study doping of oxides reaches its limit in the present case. Secondary phases as expected in the case of unsuccessful doping are hard to detect at doping levels of 1 mol-%, and lattice parameter changes as a criteria for successful doping have to be analysed with great care in the case of nanocrystals[28,29].

Nitrogen sorption measurements give high surface area ranging between 97 m^2/g for pure CeO_2 and 92 m^2/g for the Pt-doped samples. The values were determined using the BET method. Due to the poor morphological stability of cerium oxide, the surface area significantly drops after a heat treatment at 700°C to 22 m^2/g.

3.2 Catalytic Tests

CO oxidation using molecular oxygen O_2 was carried out over freshly prepared and reduced samples containing 1 mol% Pt. The CO conversion over temperature (light-off curve) for the as-synthesized, 300°C, 500°C and 700°C hydrogen-treated samples are shown in Figure 2a. In comparison to the activity of the as-synthesized samples (T_{50} = 240°C; T_{50} is the temperature where 50% conversion is reached), conversion of CO takes place at much lower temperatures after hydrogen treatment at 300°C and 500°C (T_{50} = 46°C and 109°C). After treatment at 700°C, the performance drops further (T_{50} =180°C). The influence of the different pre-treatment temperatures on the catalytic activity points to a strong influence of the oxidation state of the platinum species and interaction with the ceria support. The reactivity of the sample treated at 300°C under hydrogen is remarkable, as it converts CO already at room temperature. Consequently, we also studied deactivation of this sample at 30°C, 45°C and 60°C. We changed the test conditions to be closer to the conditions of air treatment, that is lower CO concentration (2000 ppm) and higher GHSV (400 000h^{-1}). Under isothermal conditions, the initial performance of 10% CO conversion (30°C), 23% CO conversion (45°C) and 26% CO conversion (60°C) decreases to 3% conversion, 5% conversion and 12% conversion after 80 minutes on stream (Figure 2b). The initial deactivation of platinum-based catalysts in CO oxidation is not surprising, since CO is also an inhibitor for platinum catalysts at low temperatures [30]. Even though the CO conversion after 80 minutes seems to be quite low, still 60 ppm of CO are converted at 30°C, 100 ppm at 45°C and 240 ppm at 60°C. In the context of air depollution, the targeted pollution concentration is usually below 100 ppm or even at the ppb level, showing the potential of these catalysts at ambient temperatures.

3.3 HRTEM and HAADF-STEM analysis

HRTEM and HAADF-STEM micrographs of as-synthesized and pretreated 1%Pt_CeO_2 samples are shown in Figure 3. The ceria crystallites are agglomerated and irregular in shape, so various crystalline planes are exposed on the surface. The crystallite size of the cerium oxide particles can be determined using HRTEM analysis (Figure 3 a) and vary between 6 and 10 nm, which is in agreement to the results obtained from XRD measurements (for further images, see also Supporting Information, SI1).

HAADF-STEM analysis allows for a better contrast between platinum nanoparticles and ceria. The as-synthesized sample and the one treated at 300°C do not show platinum nanoparticles on the surface, indicating successful integration of Pt in the cerium oxide lattice. However, for the latter the formation of metallic Pt surface atoms cannot be excluded. After hydrogen treatment at 500°C, first small Pt particles become visible. These particles appear more pronounced after hydrogen treatment at 700°C, with a Pt-nanoparticle size of 2 nm in size. The ex-solution of noble metal nanoparticles from doped ceria using hydrogen is well-documented in the literature[11,21] and can be considered as a method do obtain a homogeneous distributed catalyst. However, in our case, the best performing catalyst is the one after hydrogen treatment at 300°C. In this case, we do not observe clearly defined nanoparticles, but the presence of isolated surface Pt atoms cannot be entirely excluded (see also XPS Figure 4b). Whether platinum atoms and/or segregated structures play a role in the catalytic performance is difficult to proof.

3.4 Surface characterization: X-Ray Photoelectron Spectroscopy, H_2 – chemisorption and TPR

XPS experiments of the Pt(4f) core level region were carried out on one-step synthesized samples treated at different temperatures under hydrogen. For reference, pure PtO_2 and Pt-foil were also measured. The spectra were corrected for charging effects using the carbon C(1s) peak at 284.8 eV.

XPS of the Pt(4f) core level region in as-prepared and heat-treated 1%Pt_CeO_2 are shown in Figure 4. The Pt(4f) region shows the presence of multiple oxidation states of Pt. It can be deconvoluted into three pairs of spin-orbit doublets. The Pt($4f_{7/2}$) and Pt($4f_{5/2}$) can be attributed to metallic (Pt^0: 70.5 and 73.8 eV), divalent (Pt^{2+}: 72.0 and 75.2 eV), and tetravalent (Pt^{4+}: 73.7 and 76.9 eV) oxidation states. The amount of Pt^0, Pt^{2+} and Pt^{4+} present in the samples were estimated from the XPS spectra (see Table 2). The relative intensities vary strongly with the reducing conditions. Even though the values are very approximate, a general trend towards

the formation of Pt^0 with increasing reduction temperature can be observed. Significant amount of oxidized platinum can be found even after reduction at 700°C, which is probably due to reoxidation of the highly dispersed Pt nanoparticles. The concentration of platinum determined by XPS is remarkable low (Pt/Ce varies between 0.0056 and 0.0119). From elemental analysis (see Supporting Information, SI2), the platinum content is 1.03 mol % and thus close to the expected value. This hints towards successful doping of Pt inside the cerium oxide lattice. With increasing pre-treatment temperature, the Pt/Ce ratio increases, this indicates that Pt is accumulated on the surface through the treatment under hydrogen.

When comparing the catalytic activity of the different samples to the oxidation state as obtained from XPS analysis, ionic platinum apparently plays a role in the catalytic activity. The samples heated at 300°C under hydrogen show the best CO conversion activity, and most platinum is present in the oxide form. However, XPS is not sufficient to explain the observed differences between the different pre-treatment temperatures. In order to further study the availability of platinum on the catalyst surface, H_2-chemisorption measurements after hydrogen pretreatment at 300 °C are presented in Figure SI3. The experiment was carried out at -77°C to avoid hydrogen spillover to ceria. According to the measurement, the platinum metal dispersion is 11%, which corresponds to a particle size of 10 nm in the case of a Pt concentration of 1 mol%. This result would be in disagreement with the results from HAADF-STEM analysis, which reveal no pronounced particles on the surface after hydrogen treatment at 300°C. Therefore, this experiment demonstrates that not all platinum is located on the surface and the particle size cannot be determined using H_2-chemisorption. The result supports the idea of ceria doping with platinum, with only minor platinum segregated on the surface.

Another tool to study interaction between ceria and platinum is temperature programmed reduction under hydrogen. The TPR profiles up to 900°C of 1% Pt_CeO_2 and pure ceria are shown in Figure 5. Pure ceria shows the typical features of a high surface area material, that is reduction of surface ceria at moderate temperature (380-600°C) and bulk reduction at higher temperature (from 650°C) [31]. In the presence of platinum, we find a strong H_2 consumption peak at 138 °C, a broad and weak H_2 consumption peak at 440°C and finally the bulk reduction peak starting from 640°C. Thus, the reduction features of ceria are altered in the presence of platinum. The strong reduction peak at 138 °C demonstrates the combined reduction of platinum and surface ceria species in vicinity to the metal [21,32]. This result suggests that some platinum is at least partially reduced, as already seen by XPS measurements. The observation that also ceria reduces during the H_2-pretreatment should not further affect the catalytic performance of the catalyst. It has been shown in the literature that active Ce^{3+} are

short-lived and do not contribute to the catalytic performance under steady-state conditions[33]. Also, we carried out the H_2 pretreatment separated from the CO oxidation experiment, leaving the catalyst on air for one week. The ex-situ treated catalyst shows similar performance to the in-situ treated catalyst.

X-Ray Absorption Fluorescence Spectroscopy

The normalized Pt L_{III}-edges XANES (X-ray absorption near edge spectroscopy) of one-step synthesized catalysts are shown in Figure 6. The absorption edge energy E_0 is determined from the first maxima in the derivative spectrum (see Figure 6b). As references, the XANES and derivative spectra of platinum metal (E_0=11 564 eV) and PtO_2 (E_0=11 568 eV) are shown as well. The trend in changes in the white line with increasing hydrogen treatment temperature is clearly pronounced: the edge energy of the as-synthesized sample is the very close to PtO_2 (11 567 eV) and decreases with increasing temperature (11 565 eV for 300°C, 11 565eV for 500°C and 11 564eV for the 700°C sample). The shift of the edge energy is illustrated in Figure 6 b (derivative spectra of the normalized XANES spectra).

The white line intensity (intensity of the Pt L_{III}-adsorption edge) changes upon heat treatment under hydrogen. The white line intensity is directly related to the electronic transition from occupied 2p orbitals to unoccupied 5d orbitals and accounts for the oxidation state of the platinum species[34]. The high oxidation state of the one-pot as-synthesized sample is due to the oxidizing synthesis conditions (decomposition of nitrates) and shielding of the platinum via the surrounding cerium oxide. Even though the white line intensity strongly decreases when going from the as-synthesized sample to the samples treated at 300°C, 500°C and 700°C, it remains slightly higher than the white line intensity of Pt-metal. This indicates that some platinum remains oxidized after the reduction treatment at 700°C, which is in accordance with the results from XPS. The observation that platinum nanoparticles remain slightly oxidized when deposited on nanosized ceria can be due to surface oxidation of the platinum nanoparticles. In addition, it has been shown by several groups that nanosized platinum deposited on nanosized ceria strongly interacts with the ceria support via oxygen transfer to the platinum nanoparticles and/or shared oxygen between the support and platinum.[35–37]

The k^3-weighted Fourier transformations (FT) of the EXAFS (extended X-ray absorption fine structure) signal for PtO_2 and platinum are shown in Figure 7, and the FT of the one-step synthesized samples are shown in Figure 8 (for details on the Pt-O and Pt-Pt contribution to the fit see Supporting Information, SI4). The FTs were performed at the Pt L_{III}-edge EXAFS spectra

in the 2-12 $Å^{-1}$ region. The quantitative fitting analysis of the EXAFS spectra was done using Artemis. The EXAFS data were fitted using several models, such as Pt metal, PtO_2 and for the one-step derived samples also solid solution models substituting Ce^{4+} with Pt^{4+} in the cerium lattice. The structural information (bond distance, coordination number, and Debye-Waller factors) obtained from EXAFS analysis of references (Pt-metal and PtO_2) and samples are summarized in Table 3 and Table 4. The FTs shown in Figure 7 and Figure 8 are not corrected for phase shifts, the peaks are thus shifted to lower R-values when compared to the exact R-values shown in Table 3 and 4 obtained from curve fitting.

Regarding the FT of PtO_2 and Pt-metal, the peaks corresponding to Pt-O and Pt-Pt (2.00 Å and 3.08 Å in Table 6, respectively) are indicated in Figure 6a. For Pt foil, the peak at 2.76 Å (Table 6) is related to Pt-Pt bond.

In all analysed samples, a correlation distance at 2.00 Å can be found, which can be attributed to the Pt-O bond in PtO_2. While the coordination number for this distance decreases with increasing treatment temperature, we always find a significant contribution from oxidized platinum. The coordination number (CN) of the Pt-O shell in the one-pot as-synthesized sample is 4.6, indicating oxygen rich surrounding around Pt. At the same time, the CN is relatively low considering the fact the coordination of ceria to oxygen is eight. One should interpret this number with care, since the error related to this value is relatively high and in general difficult to fit accurately.[38] Second, in our case we have nanosized ceria with numerous defaults on the surface. Also, we do not have information about the homogeneity of the sample. The low CN hints towards platinum located close to the surface of the nanoparticles, in a vacancy rich environment. The second peak in the as-synthesized 1%Pt_CeO_2 sample does not match entirely with the Pt-O-Pt correlation of PtO_2. Therefore, curve-fitting analysis was performed based on the assumption that Ce as second neighbour atom contributes to the spectrum. Figure 8 shows the FTs of as-synthesized one-pot sample along with the fits and corresponding Pt-O, Pt-Pt and Pt-Ce contributions. The fit of the one-pot sample can be significantly improved by including Pt-Ce contributions. Therefore, we can account for the true doping of Pt inside the lattice of cerium oxide for the as-synthesized one-pot sample. This doping is stable after hydrogen treatment at 300°C, where Pt-Ce contributions are still present. In contrast to surface sensitive characterization method, we do not observe metallic platinum in the sample treated at 300°C under hydrogen. One has to keep in mind that EXAFS is an analysis technique giving an average value over the whole sample. Since the contribution of metallic platinum is very low, it might not be detected using EXAFS. The situation changes completely after hydrogen

treatment at 500°C: we observe significant contribution from metallic platinum, indicating the migration of Pt towards the cerium oxide surface. This is in coherence with observations from HAADF-STEM analysis (presence of Pt nanoparticles at the surface after 500°C treatment).

4. Conclusion

In this work, we study the catalytic activity of platinum-cerium oxide catalysts in the light of oxidation state of the catalytic active species and integration in the cerium oxide support. The catalysts were synthesized in one-step in order to integrate the platinum in the lattice (doping). The successful doping of cerium oxide with platinum is confirmed using EXAFS. The catalysts were pre-treated under hydrogen at different temperatures (300°C, 500°C and 700°C) to tune the oxidation state of platinum. The so-prepared samples are characterized by their high surface area (higher than 90 m^2/g) and small platinum particle size in case of ex-soluted platinum (2 nm). Compared to other synthesis routes reported in the literature, the here described synthesis method strikes out due to the simplicity of the procedure: platinum-doped ceria with high surface area can be synthesized by simple slow decomposition of the nitrate precursors, where the degradation of the precursors starts at temperatures as low as 180°C.

The idea of the one-step synthesized sample is to actually dope cerium oxide with platinum while keeping a high surface area of cerium oxide. Doping of cerium oxide with platinum has been proposed to improve the cerium oxide properties as catalyst support[25]. As seen from XAFS analysis, doping was achieved for the as-synthesized sample and is stable after hydrogen treatment at 300°C. The Pt-Ce contribution changes upon hydrogen treatment at higher temperatures (500°C), which is further confirmed by HAADF-STEM analysis (appearance of platinum nanoparticles on the surface).

To determine the decisive role of noble metal inserted into a ceria lattice is a real challenge. Next to fully doped ceria, the noble metal can be partially doped into the ceria lattice and assembled as nanostructures on the surface, as it might also be the case for the here described system. Even in the case of true doping, the sample might not be homogeneous, but Pt might be located close to the surface. Our EXAFS data hint towards doped Pt located close to the surface. The reduction step at 300°C under hydrogen plays a significant role to improve the catalytic performance. The sample treated at 300°C shows the best catalytic performance, converting 7% of CO (420 ppm) at 30°C under the described conditions. From XPS and XAFS analysis, we can state that the majority of the platinum present in these samples is in an oxide

form. However, the presence of surface metallic platinum species cannot completely be ruled out (XPS data, H_2-chemisorption). In systems with several possible active sites it is difficult to differentiate between catalytic active species and spectator species. The low temperature activity of this catalyst might be due to a combination of the two: slight reduction of the platinum ceria catalyst can offer anchoring adsorption sites for CO, while the oxidised species hint towards strong interaction with the ceria support and a possibility for oxygen supply in the reaction, via a reverse spill-over. Oxygen reverse spillover between platinum nanostructures deposited on nano-sized ceria has been recently demonstrated experimentally and theoretically [36]. To further elucidate the role of the Pt in the catalytic reaction, in-situ studies using a combination of analytical tool (DRIFT, EXAFS) will be necessary.

The catalytic performance of the one-step synthesized samples is remarkable considering the fact that not all of the platinum can be found on the ceria surface, as also seen by XPS analysis. Some of the platinum integrated in the lattice might actually be shielded by the cerium oxide and thus does not interact with the reactants as active catalyst. The combination of a simple synthesis and activation protocol for platinum ceria catalysts might be used in the future to explore low temperature applications for this class of materials.

AUTHOR INFORMATION

Corresponding Author

*Helena Kaper
Ceramic Synthesis and Functionalization Laboratory
UMR 3080
Saint-Gobain CREE
550, Ave Alphonse Jauffret
84306 Cavaillon
France
Tel: (+33) 4 32 50 08 95
e-mail: helena.kaper@saint-gobain.com

References

[1] H.S. Gandhi, G.W. Graham, R.W. McCabe, J. Catal. 216 (2003) 433–442. doi:10.1016/S0021-9517(02)00067-2.

[2] X. Cheng, Z. Shi, N. Glass, L. Zhang, J. Zhang, D. Song, Z. Liu, H. Wang, J. Shen, J. Power Sources. 165 (2007) 739–756. doi:10.1016/j.jpowsour.2006.12.012.

[3] W.D. Deng, M. Flytzani-Stephanopoulos, Angew. Chem. Int. Ed. Engl. 45 (2006) 2285–2289.

[4] S. Wang, H.M. Ang, M.O. Tade, Environ. Int. 33 (2007) 694–705. doi:10.1016/j.envint.2007.02.011.

[5] J.M. Thomas, J. Chem. Phys. 128 (2008) 182502.

[6] A. Neitzel, A. Figueroba, Y. Lykhach, T. Skála, M. Vorokhta, N. Tsud, S. Mehl, K. Ševčíková, K.C. Prince, K.M. Neyman, V. Matolín, J. Libuda, J. Phys. Chem. C. 120 (2016) 9852–9862. doi:10.1021/acs.jpcc.6b02264.

[7] L. Nie, D. Mei, H. Xiong, B. Peng, Z. Ren, X.I.P. Hernandez, A. DeLaRiva, M. Wang, M.H. Engelhard, L. Kovarik, A.K. Datye, Y. Wang, Science 358 (2017) 1419–1423. doi:10.1126/science.aao2109.

[8] J. Johnes, H. Xiong, A.T. DeLaRiva, E.J. Peterson, H. Pham, S.R. Challa, G. Qi, S. Oh, M.H. Wiebenga, X.I. Pereiera Hernandez, Y. Wang, A.K. Datye, Science 353 (2016) 150–154.

[9] F. Gao, Y. Cai, K.K. Gath, Y. Wang, M.S. Chen, Q.L. Guo, D.W. Goodman, J. Phys. Chem. 113 (2009) 182–192.

[10] F.J. Gracia, L. Bollmann, E.E. Wolf, J.T. Miller, A.J. Kropf, J. Catal. 220 (2003) 382–391. doi:10.1016/S0021-9517(03)00296-3.

[11] L.M. Misch, J.A. Kurzman, Chem. Mater. 23 (2011) 5432–5439.

[12] Q. Fu, H. Saltsburg, M. Flytzani-Stephanopoulos, Science 301 (2003) 935–8. doi:10.1126/science.1085721.

[13] D.A.J.M. Ligthart, R.A. Van Santen, E.J.M. Hensen, Chem. Commun. (2011) 5306–5310. doi:10.1002/anie.201100190.

[14] W.F. Libby, Science 171 (1971) 499.

[15] R.J.H. Voorhoeve, D.W. Johnson, P.K. Remeika, P.K. Gallagher, Science 195 (1977) 827–833.

[16] T. Baidya, A. Gupta, P.A. Deshpandey, G. Madras, M.S. Hegde, J. Phys.Chem. C. (2009) 4059–4068.

[17] M.S. Hegde, G. Madras, K.C. Patil, Acc. Chem. Res. 42 (2009), 704-712.

[18] S. Roy, M.S. Hegde, Catal. Commun. 9 (2008), 811–815. doi:10.1016/j.catcom.2007.09.019.

[19] P. Bera, S. Malwadkar, A. Gayen, C.V. V Satyanarayana, B.S. Rao, M.S. Hegde, Catal. Lett. 96 (2004), 213-219.

[20] R. V Gulyaev, T.Y. Kardash, S.E. Malykhin, O. A. Stonkus, A. S. Ivanova, A. I. Boronin, Phys. Chem. Chem. Phys. 16 (2014) 13523–39. doi:10.1039/c4cp01033g.

[21] M. Kurnatowska, L. Kepinski, W. Mista, Appl. Catal. B Environ. 117–118 (2012) 135–147. doi:10.1016/j.apcatb.2011.12.034.

[22] P. Singh, M.S. Hegde, C, J. Solid State Chem. 181 (2008) 3248–3256. doi:10.1016/j.jssc.2008.08.018.

[23] C.I. Hiley, J.M. Fisher, D. Thompsett, R.J. Kashtiban, R.I. Walton, 21 (2015) 13072–13079. doi:10.1039/C5TA02007G.

[24] D.O. Scanlon, B.J. Morgan, G.W. Watson, Phys. Chem. Chem. Phys. 13 (2011) 4279–84. doi:10.1039/c0cp01635g.

[25] W. Tang, Z. Hu, M. Wang, G.D. Stucky, H. Metiu, E.W. McFarland, J. Catal. 273 (2010) 125–137. doi:10.1016/j.jcat.2010.05.005.

[26] D.A. Shirley, Phys. Rev. B Condens. Mater. Phys. 1972, 5, 4709. 5 (1972) 4709.

[27] J.H. Scofield, J. Electron. Spectros. Relat. Phenom. 8 (1976) 129.

[28] B. Palosz, E.I. Grzanka, S.I. Gierlotka, S.I. Stel, R.I. Pielaszek, U.Bismayer, J. Neuefeind, H.-P. Weber, Th. Proffen, R. Von Dreele, W. Palosz. Z. Kristallogr. 217 (2002) 497–509.

[29] B. Palosz, E. Grzanka, S. Gierlotka, S. Stelmakh, Z. Kristallogr. 225 (2010) 588–598. doi:10.1524/zkri.2010.1358.

[30] S.E. Voltz, C.R. Morgan, D. Liederman, S.M. Jacob, Ind. Eng. Chem. Prod. Res. Develop. 12, (1973) 294-301.

[31] F. Giordano, A. Trovarelli, C. De Leitenburg, M. Giona, J. Catal. 282 (2000) 273–282. doi:10.1006/jcat.2000.2900.

[32] B.B. Harrison, A.F. Diwell, C. Hallett, Platinum Metals Rev. 32, (1988) 73–83.

[33] R. Kopelent, J. a. van Bokhoven, J. Szlachetko, J. Edebeli, C. Paun, M. Nachtegaal, O. V. Safonova, Angew. Chemie Int. Ed. 54 (2015) 8728–8731. doi:10.1002/anie.201503022.

[34] A.N. Mansour, J.W. Cook, D.E. Sayers, J. Phys. Chem. 88 (1984) 2330–2334.

[35] S. Gatla, D. Aubert, G. Agostini, O. Mathon, S. Pascarelli, T. Lunkenbein, M.G. Willinger, H. Kaper, ACS Catal. 6 (2016) 6151–6155. doi:10.1021/acscatal.6b00677.

[36] M. Cargnello, V.V.T. Doan-Nguyen, T.R. Gordon, R.E. Diaz, E.A. Stach, R.J. Gorte, P. Fornasiero, C.B. Murray, Science 341 (2013) 771–773.

[37] G.N. Vayssilov, Y. Lykhach, A. Migani, T. Staudt, G.P. Petrova, N. Tsud, T. Skála, A. Bruix, F. Illas, K.C. Prince, V. Matolín, K.M. Neyman, J. Libuda, Nat. Mater. 10 (2011) 310–5. doi:10.1038/nmat2976.

[38] H. Deguchi, H. Yoshida, T. Inagaki, M. Horiuchi, Solid State Ionics. 176 (2005) 1817–1825. doi:10.1016/j.ssi.2005.04.043.

Table captions

Table 1. Lattice parameter, crystallite size and surface area of the one-pot 1% Pt_CeO_2 samples treated at different temperatures under hydrogen.

Table 2. The percentage of Pt^{4+}, Pt^{2+} and Pt^0 in Pt_CeO_2 and 1%Pt_CeO_2 reduced at different temperature as determined from deconvulated XPS analysis.

Table 3. Structural parameters of k^3-weighted EXAFS spectra of Pt-metal and PtO_2.

Table 4. Structural parameters of k^3-weighted EXAFS spectra at the Pt-L_3-edge of Pt supported samples prepared by one-step synthesis after different reduction treatments.

Figure captions

Fig. 1. XRD pattern of the one-step synthesized samples treated under hydrogen at different temperatures.

Fig. 2. a) CO conversion versus temperature curves of the one-step synthesized samples treated under hydrogen at 300°C, 500°C and 700°C. b) CO oxidation performance at low temperature using 25mg of pretreated catalyst and 2000 ppm of CO.

Fig. 3. HRTEM and HAADF-STEM images of 1%Pt_CeO_2. a) as-synthesized, b), c), d) treated at 300°C under H_2, e) treated at 500°C under H_2 and f) treated at 700°C under H_2. The insets in a) denote a power spectrum of the region of interests corresponding to CeO_2.

Fig. 4. XPS spectra of a) impregnated and b) one-step synthesized samples treated at 300°C, 500°C and 700°C under H_2.

Fig. 5. Temperature-programmed reduction under hydrogen for 1%Pt_CeO_2 (black curve) and pure ceria (red curve). Prior to the test, the samples were treated under oxygen at 350°C to eliminate surface carbonates.

Fig. 6. a) a) Normalized XANES spectra at Pt L_{III}-edge of Pt-foil, PtO_2, 1%Pt_CeO_2_as, 1%Pt_CeO_2_300H_2 , 1%Pt_CeO_2_500H_2 and 1%Pt_CeO_2_700H_2. b) derivative spectra of a).

Fig. 7. Fourier transformed (FT) k^3-weighed data of Pt L_{III}-edge EXAFS for PtO_2 and Pt foil. Dotted lines correspond to fits.

Fig. 8. FT of one-step synthesized samples, as-synthesized and treated under hydrogen at 300°C, 500°C and 700°C. Dotted lines correspond to fits.

Tables

Table 1. Lattice parameter, crystallite size and surface area of the one-pot 1% Pt on CeO_2 samples treated at different temperatures under hydrogen.

	reduction temperature/°C	lattice parameter / Å	crystallite size / nm	surface area / m^2/g
CeO_2		5.4125	9	97
1%Pt_CeO_2		5.4114	10	92
	300	5.4135	10	92
	500	5.4133	8	84
	700	5.4104	31	22

[a] The surface area was determined by using nitrogen physisorption measurements and the Brunauer-Emmett-Teller method (BET).

Table 2. The percentage of Pt^{4+}, Pt^{2+} and Pt^{0} in Pt_CeO_2 and 1%Pt_CeO_2 reduced at different temperature as determined from deconvulated XPS analysis.

	Pt^{4+}	Pt^{2+}	Pt^{0}	Pt/Ce
1%Pt_CeO_2_as	10	74	16	0.0056
1%Pt_CeO_2_300 H_2	0	82	18	0.0072
1%Pt_CeO_2_500 H_2	8	56	36	0.0119
1%Pt_CeO_2_700 H_2	15	42	43	0.0086

Table 3. Structural parameters of k^3-weighted EXAFS spectra of Pt-metal and PtO_2

Sample	**Shell**	**CN**	**R(Å)**	**σ^2(Å^{-2})**	**ΔEo / eV**
PtO_2	Pt-O	4.8 ± 0.6	2.00 ± 0.01	0.003 ± 0.001	11 ± 1
	Pt-Pt	4.8	3.08 ± 0.01	0.008 ± 0.004	
Pt foil	Pt-Pt	12.0	2.764 ± 0.002	0.0049 ± 0.0001	8.5 ± 1
	Pt-Pt	6.0	3.92 ± 0.01	0.007 ± 0.001	

CN: coordination number, R: coordination distance, σ^2: Debye-Waller factor

Table 4. Structural parameters of k^3-weighted EXAFS spectra at the Pt-L_3-edge of Pt supported samples prepared by one-step synthesis after different ex-situ reduction treatments.

Sample	**Treatment**	**Shell**	**CN**	**R/Å**	**σ^2 / Å^2**	**ΔE**
1%Pt_CeO_2	as-synthesized	Pt-O	4.6 ± 0.4	2.00 ± 0.01	0.0014 ± 0.001	11 ± 2
		Pt-Pt	3.7 ± 1.2	3.09 ± 0.05	0.009 ± 0.003	
		Pt-Ce	2.3 ± 1.2	3.16 ± 0.04	0.009 ± 0.003	
	300°C/H_2	Pt-O	3.0 ± 0.5	2.00 ± 0.01	0.002 ± 0.001	12 ± 2
		Pt-Pt	3.6 ± 1.4	3.11 ± 0.04	0.010 ± 0.006	
		Pt-Ce	1.0 ± 0.3	3.21 ± 0.02	0.010 ± 0.006	
	500°C/H_2	Pt-O	2.6 ± 0.4	2.03 ± 0.02	0.006 0.002	14 ± 2
		Pt-Pt	2.6	3.12 ± 0.02	0.008 ± 0.002	
		*Pt-Pt	3.6	2.70 ± 0.02	0.013± 0.003	8.5
	700°C/H_2	Pt-O	1.0	2.03 ± 0.02	0.002 ± 0.001	14 ± 3
		*Pt-Pt	5.5 ± 1	2.70 ± 0.01	0.009 ± 0.001	8.5

CN: coordination number, R: coordination distance, σ^2: Debye-Waller factor, *Pt-Pt coordination from Pt metal phase

Figures

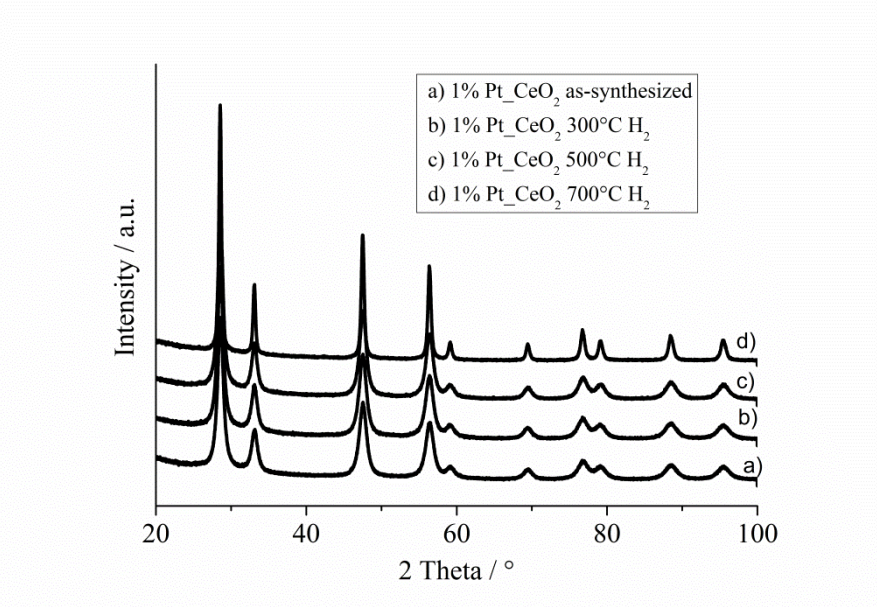

Fig. 1. XRD pattern of the one-step synthesized samples treated under hydrogen at different temperatures.

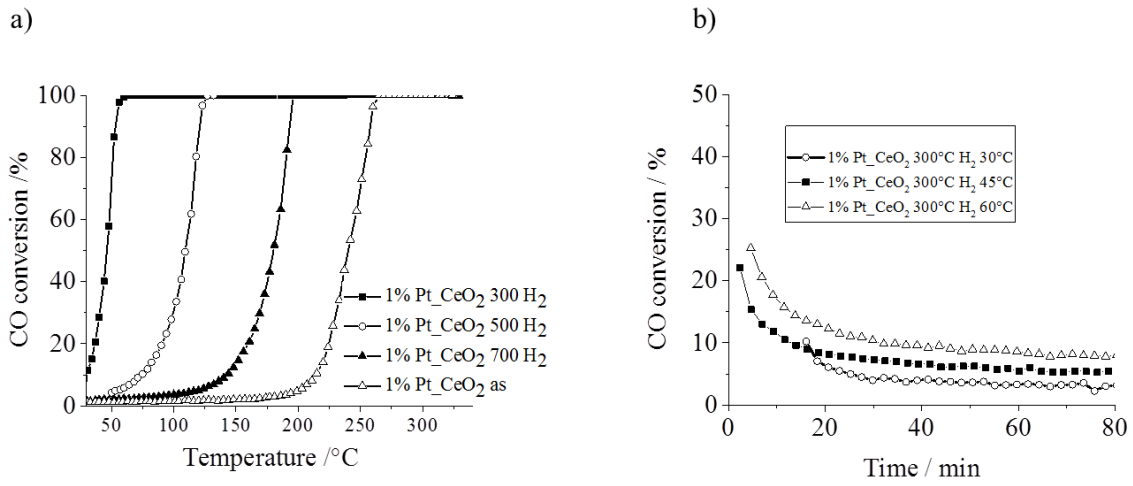

Fig. 2. a) CO conversion versus temperature curves of the one-step synthesized samples treated under hydrogen at 300°C, 500°C and 700°C, measured with a GHSV of 50 000h^{-1} b) CO oxidation performance at low temperature using 25mg of pretreated catalyst and 2000 ppm: of CO, measured with a GHSV of 400 000h^{-1}.

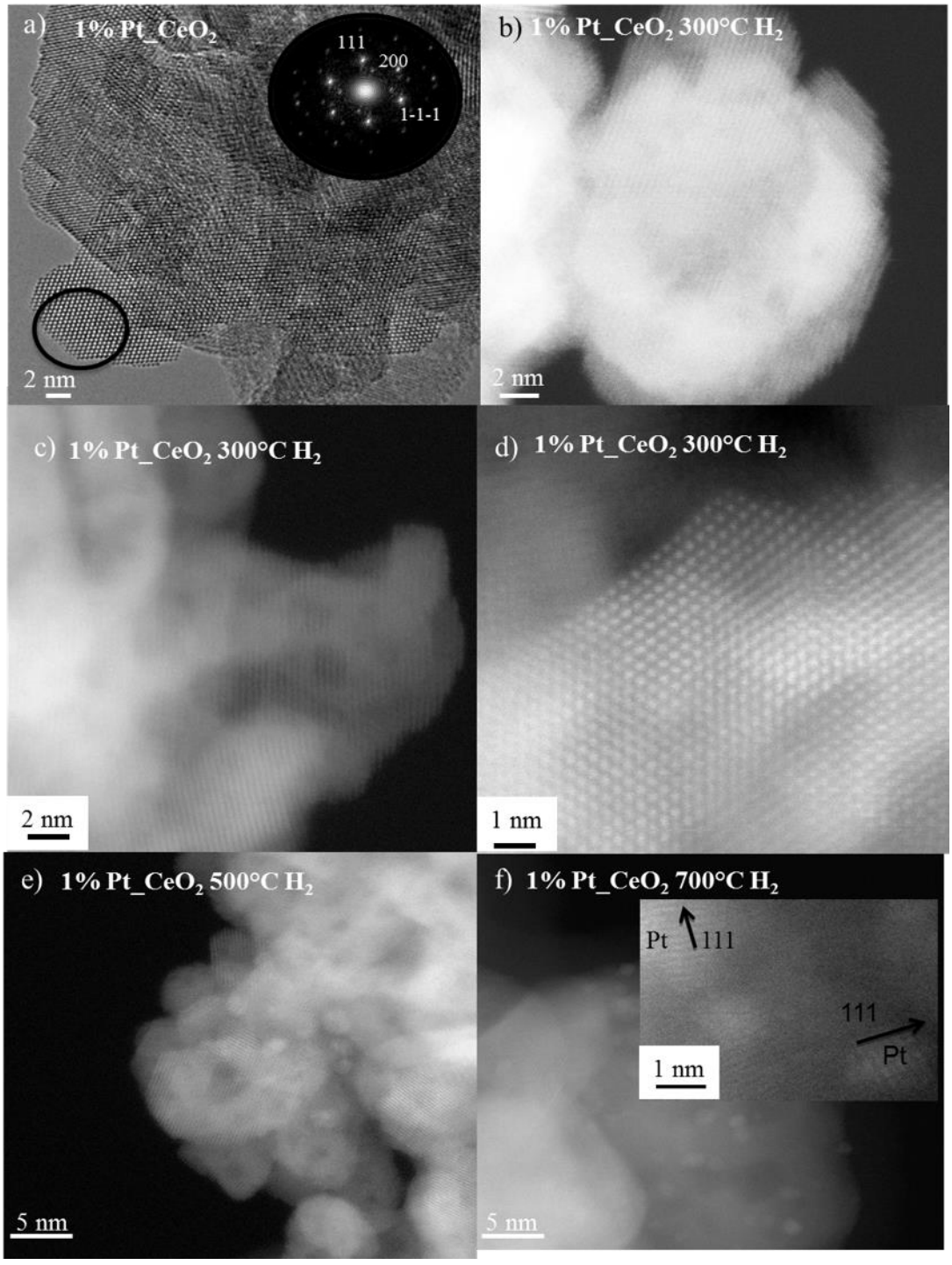

Fig. 3. HRTEM and HAADF-STEM images of 1%Pt_CeO_2. a) as-synthesized, b), c), d) treated at 300°C under H_2, e) treated at 500°C under H_2 and f) treated at 700°C under H_2. The insets in a) denote a power spectrum of the region of interests corresponding to CeO_2.

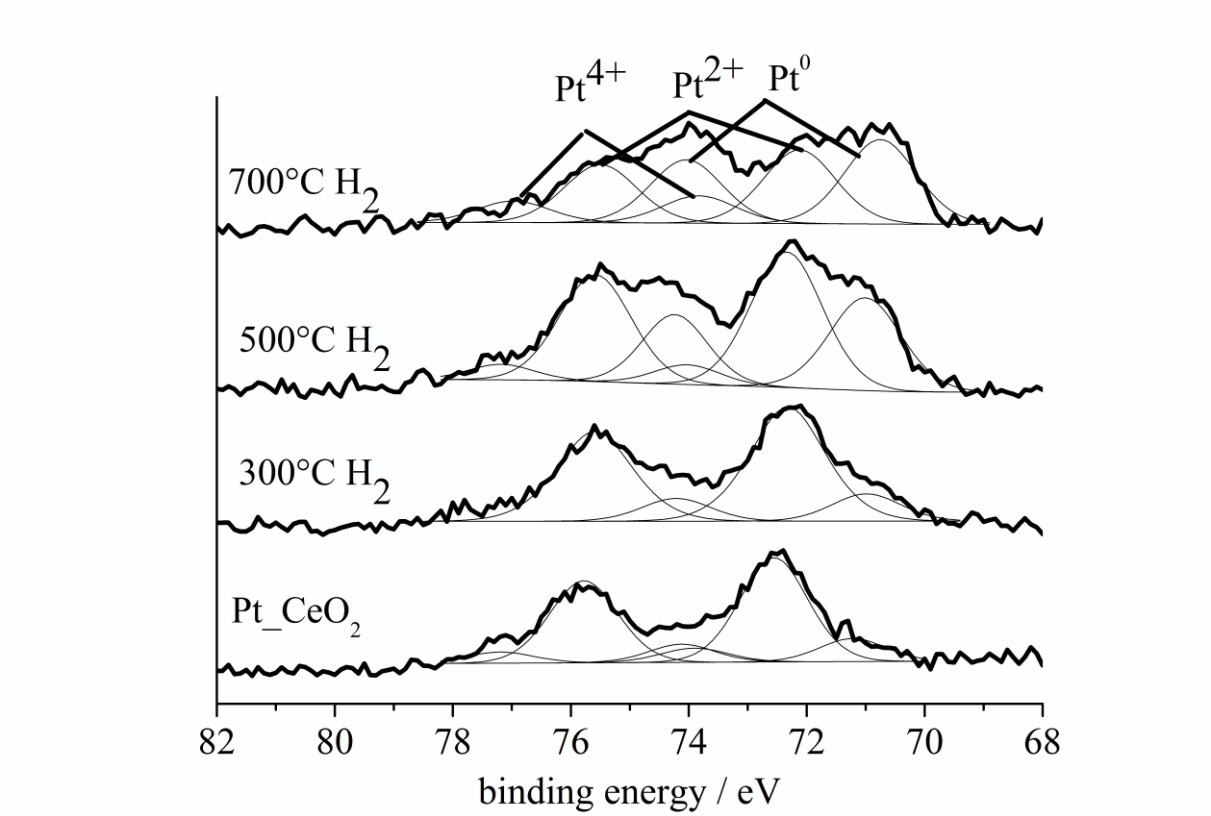

Fig. 4. XPS spectra of one-step synthesized samples treated at 300°C, 500°C and 700°C under H_2.

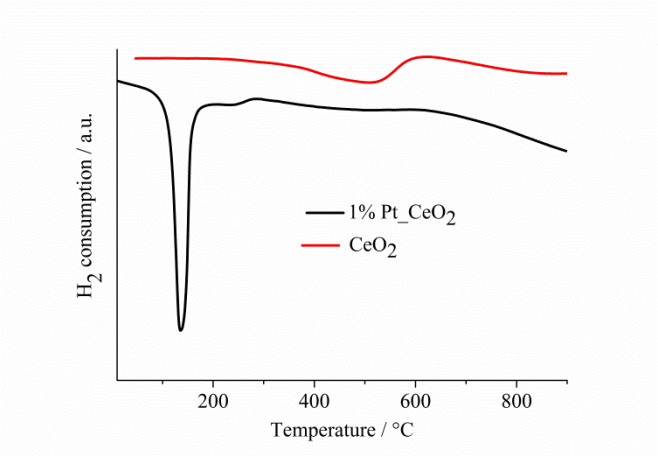

Fig. 5. Temperature-programmed reduction under hydrogen for 1%Pt_CeO_2 (black curve) and pure ceria (red curve). Prior to the test, the samples were treated under oxygen at 350°C to eliminate surface carbonates.

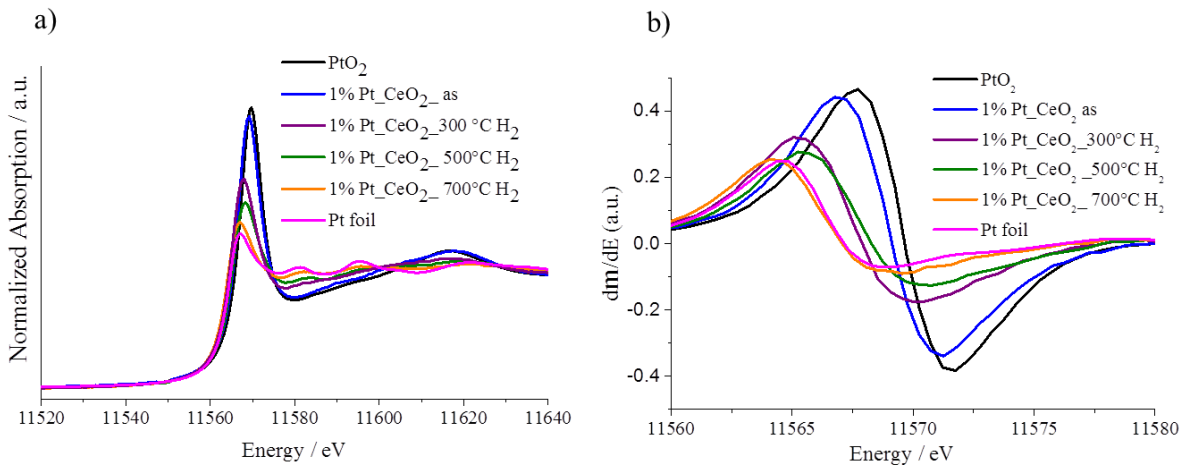

Fig. 6. a) Normalized XANES spectra at Pt L_{III}-edge of Pt-foil, PtO_2, 1%Pt_CeO_2_as, 1%Pt_CeO_2_300H_2 , 1%Pt_CeO_2_500H_2 and 1%Pt_CeO_2_700H_2. b) derivative spectra of a).

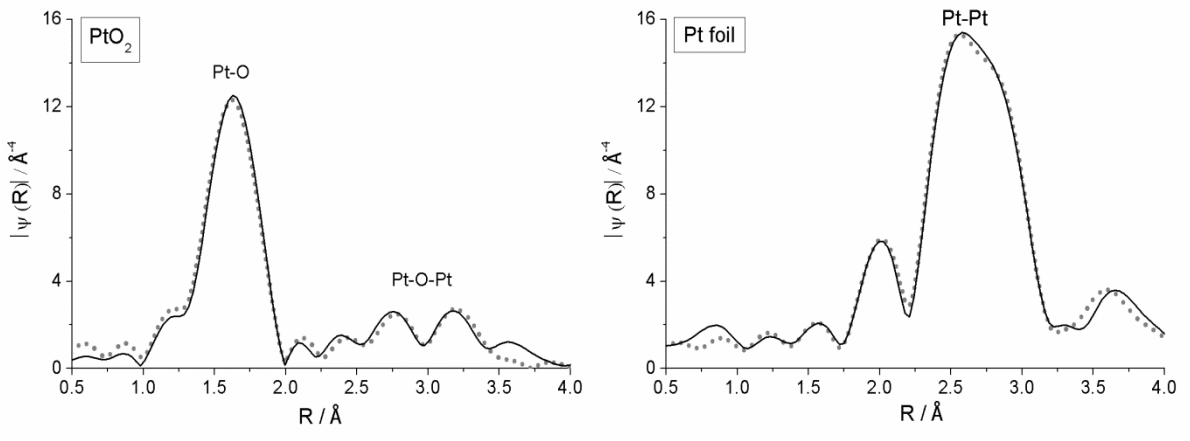

Fig. 7. Fourier transformed (FT) k^3-weighed data of Pt L_{III}-edge EXAFS for PtO_2 and Pt foil. Dotted lines correspond to fits.

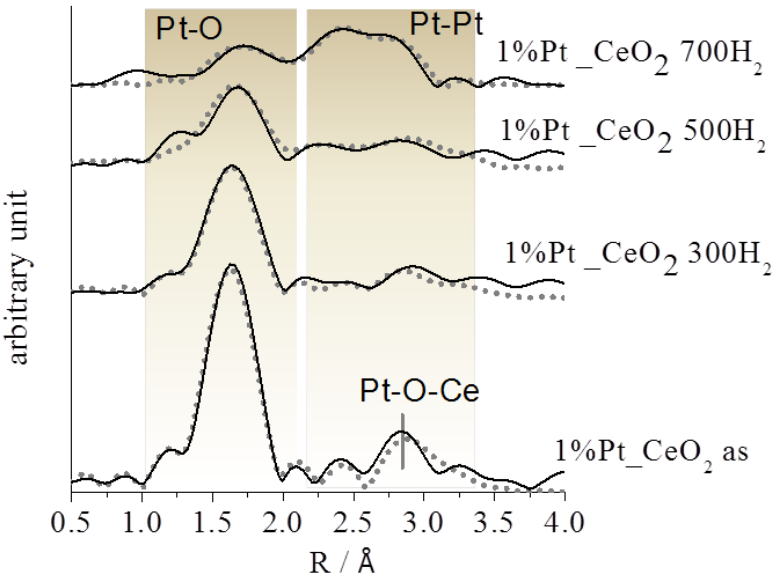

Fig. 8. FT of one-step synthesized samples, as-synthesized and treated under hydrogen at 300°C, 500°C and 700°C. Dotted lines correspond to fits.

Supporting Information

for

Facile synthesis of high-surface area platinum-doped ceria for low temperature CO oxidation

Suresh Gatla, D. Aubert, Valérie Flaud, Rémi Grosjean, Thomas Lunkenbein, Olivier Mathon, Sakura Pascarelli, Helena Kaper

SI1:
TEM images of Pt_CeO_2 and electron diffraction of the selected area.

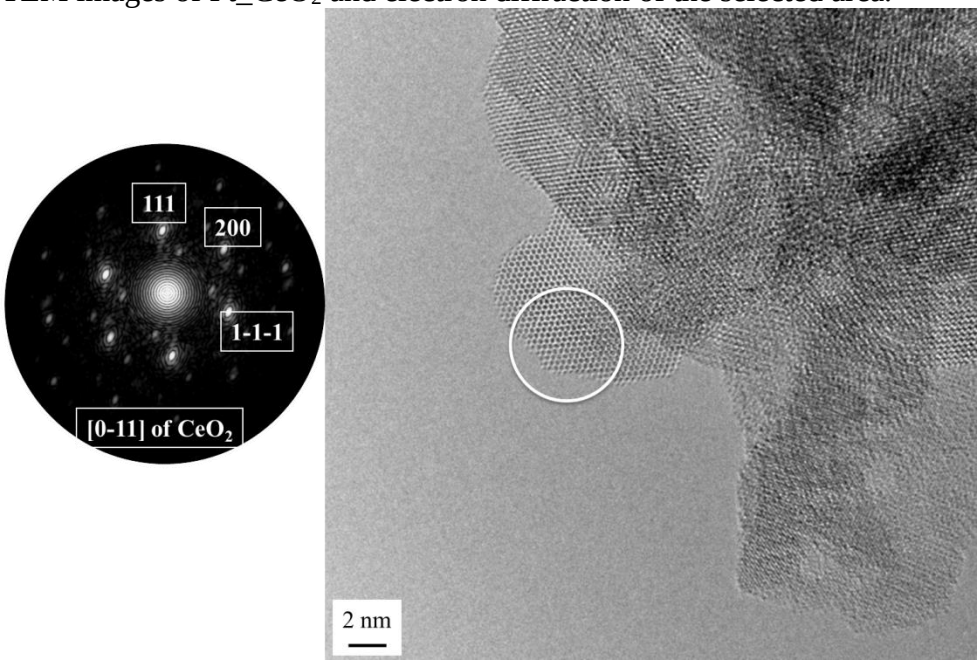

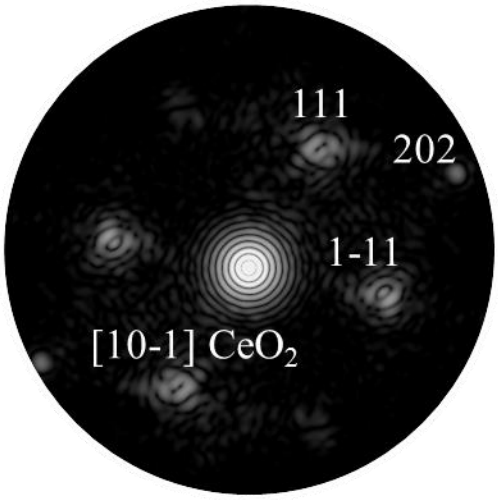

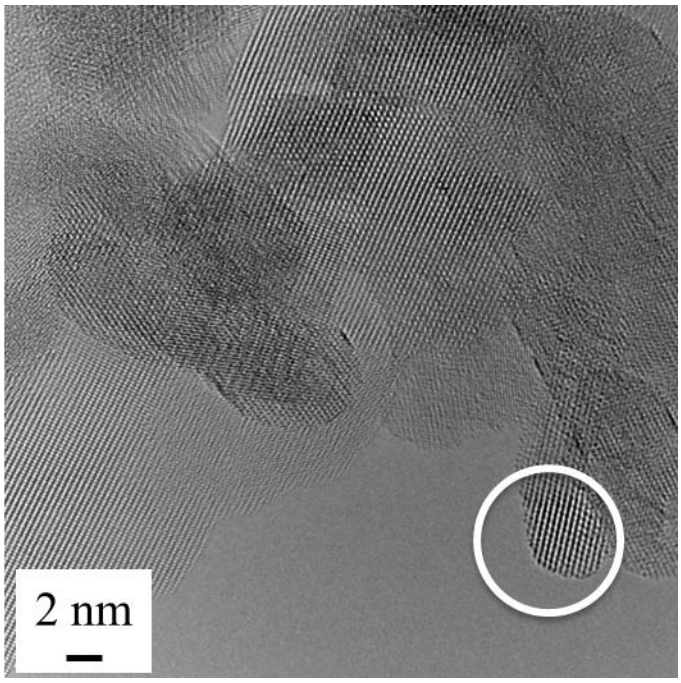

SI2:
Elemental analysis data (determined by ICP)
Pt_CeO_2: 1.03 mol-%

SI3: H_2 chemisorption of 1%Pt_CeO_2 treated at 300°C

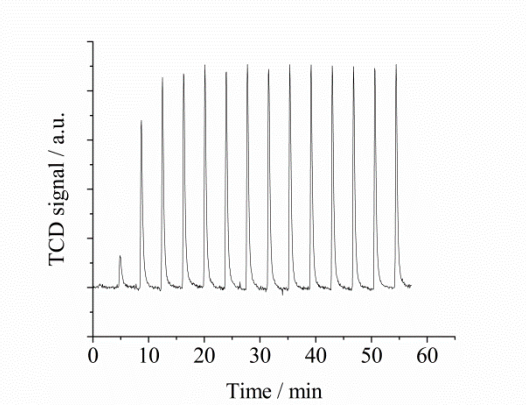

SI4:

a) b)

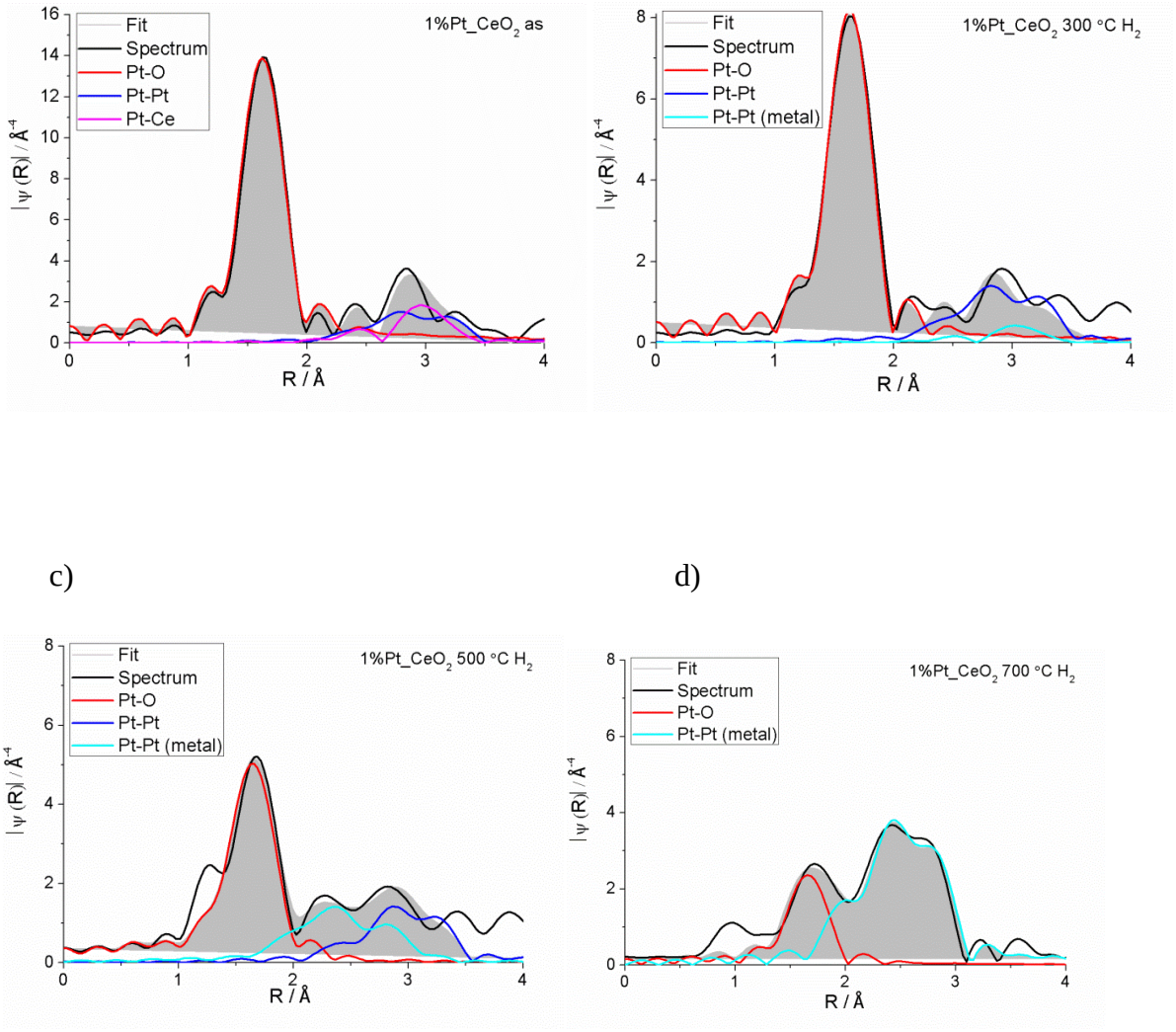

Fig. SI4: FT of as synthesized one-pot samples along with the fits (filled area) and the contributions of Pt-O, Pt-Pt, Pt-Pt (metal phase) and Pt-Ce bonds. a) as-synthesized sample; b) treated at 300°C under H_2 and c) treated at 500°C under H_2 and d) treated at 700°C under H_2.

SI5:

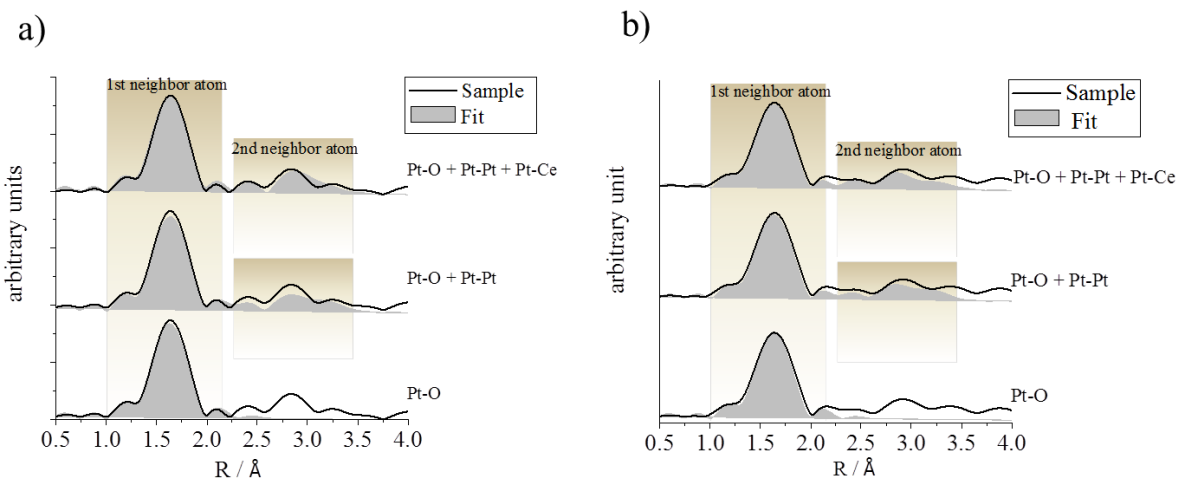

Fig. SI5 Evolution of the EXAFS fit (filled area) and FTs (solid line). a) 1% Pt_CeO_2 as-synthesized, b) 1% Pt_CeO_2 300 H_2. Contributions of Pt-O, Pt-Pt and Pt-Ce bonds are specified in the corresponding fits.